PAPER

Progress in GYRO validation studies of DIII-D H-mode plasmas

IOP Publishing and International Atomic Energy Agency Nuclear Fusion
Nucl. Fusion **52** (2012) 114007 (12pp) doi:10.1088/0029-5515/52/11/114007

Progress in GYRO validation studies of DIII-D H-mode plasmas

C. Holland[1], C.C. Petty[2], L. Schmitz[3], K.H. Burrell[2], G.R. McKee[4], T.L. Rhodes[3] and J.Candy[2]

[1] Center for Energy Research, University of California, San Diego, 9500 Gilman Drive, La Jolla, CA 92093-0417, USA
[2] General Atomics, PO Box 85608, San Diego, CA 92186-5608, USA
[3] Physics Department and PSTI, University of California, Los Angeles, PO Box 957099, Los Angeles, CA 90095-7099, USA
[4] Department of Engineering Physics, University of Wisconsin-Madison, 1500 Engineering Drive, Madison, WI 53706-1687, USA

Received 2 December 2011, accepted for publication 22 March 2012
Published 2 October 2012
Online at stacks.iop.org/NF/52/114007

Abstract
The need for a validated predictive capability of turbulent transport in ITER is now widely recognized. However, to date most validation studies of nonlinear codes such as GYRO (Candy and Waltz 2003 *J. Comput. Phys.* **186** 545) have focused upon low power L-mode discharges, which have significant differences in key dimensionless parameters such as $\rho^* = \rho_s/a$ from more ITER-relevant H-mode discharges. In order to begin addressing this gap, comparisons of the turbulent transport and fluctuations predicted by nonlinear GYRO simulations for a number of DIII-D (Luxon 2002 *Nucl. Fusion* **42** 614) H-mode discharges to power balance analyses and experimental measurements are presented. The results of two H-mode studies are presented in this paper, this first of which investigates the importance of nonlocality at typical DIII-D H-mode ρ^* values. Electrostatic global GYRO simulations of H-mode discharges at low and high rotation are shown to predict turbulence and transport levels lower than corresponding local simulations, and which are consistent with or slightly above experimental measurements and power balance analyses, even at 'near-edge' radii where gyrofluid and gyrokinetic models systematically underpredict turbulence and transport levels. The second study addresses the stabilizing effect of a significant density of energetic particles on turbulent transport. The results of local GYRO simulations of low-density QH-mode plasmas are presented, which model the fast beam ion population as a separate, dynamic ion species. The simulations show a significant reduction of transport with this fast ion treatment, which helps to understand previously reported results (Holland *et al* 2011 *Phys. Plasmas* **18** 056113) in which GYRO simulations without this treatment significantly overpredicted (by a factor of 10 or more) power balance calculations. These results are contrasted with simulations of a high-density, low fast ion fraction QH-mode discharge, which predict transport levels consistent with power balance, regardless of the fast ion treatment.

(Some figures may appear in colour only in the online journal)

1. Introduction

Accurate models of plasma transport and confinement are essential for predicting plasma performance and fusion gain in future experiments such as ITER [1] with confidence. It is therefore essential to validate these models in reactor-relevant parameter and operating regimes, namely high confinement (H-mode) plasmas, in order to establish this confidence in the model predictions of those future experiments. Absent macroscopic magnetohydrodynamic (MHD) instabilities, the dominant transport mechanism in these plasmas is so-called 'microturbulence,' which consists of a spectrum of nonlinearly interacting drift-wave instabilities [2, 3]. These instabilities are driven by the inherent free energy gradients of a confined plasma, and the turbulent eddies have characteristic cross-field correlation lengths on the order of several ion sound gyroradii $\rho_s = c_s/\Omega_{ci} (c_s = \sqrt{T_e/M_i}, \Omega_{ci} = eB/M_i c)$ or smaller. Plasma dynamics on these scales are described by the nonlinear, coupled gyrokinetic-Maxwell (GK) equations [4, 5], and a variety of numerical codes have been developed which implement these equations and solve their dynamics via different algorithms. Direct numerical solution of the GK equations remains computationally intensive when the full range of physics necessary for quantitatively meaningful predictions is retained (on the order of thousands of cpu-hours or more), and so reduced models of the drift-wave turbulence and associated transport have been developed to facilitate more computationally feasible predictions of plasma confinement. For instance, the quasilinear TGLF model [6–8] combines linear phase relations and mode structures calculated from

a seventeen-moment set of fluid equations derived from the gyrokinetic equation with a nonlinear saturation rule derived from a database of over 200 nonlinear gyrokinetic simulations performed with the GYRO code [9, 10] to predict transport and confinement properties. Using this approach, TGLF predictions of plasma confinement exhibit good agreement with observations from a variety of devices and confinement regimes, predicting incremental stored energy (i.e. within $r/a = 0.8$) to within 20% of the observations. However, full confidence in the predictions of these reduced fluid models when applied to next-generation burning plasma experiments requires detailed testing of the underlying first-principles nonlinear kinetic model against experimental observations as well.

To date, most validation studies of the nonlinear gyrokinetic code predictions have focused upon low confinement (L-mode) discharges [11–18], whereas ITER and any future reactor will need to operate using high confinement (H-mode) plasmas in order to obtain net fusion gain and power production. Given the clear quantitative and qualitative differences observed between L- and H-mode turbulence and transport properties, it is necessary to extend these validation studies to H-mode plasmas. In this work we report the results of two such investigations. The first focuses upon testing the fidelity of the gyrokinetic model in predicting energy transport and turbulence levels in so-called hybrid H-mode discharges with varying $\beta = 8\pi nT/B^2$ at low and high rotation. The results indicate that within experimental uncertainties, reasonable agreement between electrostatic turbulence simulations performed with the GYRO code and experiment is found, when global effects are retained. The definition and distinction between global and local simulations is given in section 2 below. In contrast to previous L-mode studies which have demonstrated close agreement between local and global simulation predictions, these H-mode studies find that for ITG-dominated turbulence, global gyrokinetic simulations predict transport roughly a factor of two lower than corresponding local simulations. A key difference between the L- and H-mode plasmas is that the H-modes have larger characteristic values of $\rho^* = \rho_s/a$ (where a is the midplane minor radius), due to the increased temperature values ($\rho_s \propto \sqrt{T_e}$) obtained by the increased confinement properties of the H-mode. Such a decrease in transport with increasing ρ^* is consistent with previous studies of system-size scalings of drift-wave turbulence [19–22]. For reference, typical values of ρ^* at $r/a = 0.6$ in a DIII-D L-mode is 0.0025 [14] and 0.0033 to 0.004 in the DIII-D H-modes considered in this paper, using the numerical equilibrium definitions employed in GYRO. Using these definitions, the ITER simulations presented in Kinsey *et al* [8] predict $\rho^* \sim 0.0008$ at $r/a = 0.6$.

The second study quantifies the stabilizing impact of a non-negligible density of fast ions on the microturbulence. In neutral beam-heated H-modes, particularly at lower densities, the density of residual fast beam ions that have not thermalized with the background plasma can be significant. While many previous studies have focused upon various Alfvénic instabilities which can be destabilized by this population [23–26], or upon the transport of a trace fast ion population by the plasma [27–31], significantly less attention has been paid to the stabilizing influence of the fast ion population on the turbulence [32, 33]. In previous work [18], local nonlinear GYRO simulations overpredicted transport in typical beam-heated quiescent H-modes (QH-mode) with line-averaged densities $\bar{n}_e = 2 \times 10^{13}\,\mathrm{cm}^{-3}$ by a factor of 10 or more. An improved treatment of the fast ion population was identified as a possible source of this overprediction in that paper, motivated by the observation that the fast ion density is approximately 25% of the electron density at normalized toroidal flux $r/a = 0.6$ in the plasmas considered. Including this population self-consistently within a linear growth rate calculation yielded an approximately 30% reduction in the long wavelength ITG growth rate. In this paper, we provide additional evidence that this fast ion population significantly lowers transport levels, via new local, nonlinear simulations which self-consistently include the fast ion population, and show that a factor of two reduction in transport is obtained relative to the case in which the fast ion population is neglected (or rather, treated simply as thermal ions) for the parameters considered. When electromagnetic effects are also included, transport is reduced by a factor of four to five relative to the previous undiluted, electrostatic results, bringing the predicted transport significantly closer to the levels calculated via power balance analysis.

A brief summary of the GYRO code capabilities and numerical settings are given in section 2. The comparisons to the β-scan discharges are discussed in section 3, and the QH-mode simulations in section 4. A brief discussion contrasting the generally modest overpredictions of near-edge transport (roughly $0.7 < r/a < 1$) in these H-mode simulations to robust findings of underprediction of transport by L-mode simulations at these radii is presented in section 5, and conclusions are summarized in section 6.

2. Summary of GYRO code and simulation numerics

In this work the GYRO code is used to solve the GK equations for predicted turbulence and transport levels. GYRO is a nonlinear, initial-value Eulerian code, which solves the so-called 'δf' GK equations, which describe the turbulent time and space-scale dynamics of small (order ρ^*) perturbations of the ion and electron distribution functions δf about static Maxwellian equilibrium distributions f_0. GYRO is a physically comprehensive code that includes the key physics components necessary for quantitatively accurate predictions of experimental conditions, namely realistic magnetic geometry and shaping [34], non-adiabatic electrons (both passing and trapped), like- and inter-species collisions, equilibrium rotation and flow shear, and magnetic fluctuations. Both linear and nonlinear GYRO results have been extensively verified against analytic theory and other gyrokinetic codes [6, 35, 36].

GYRO simulations can be operated in either a local or global mode. In the local mode, the rigorous $\rho^* \to 0$ limit of GK equations are solved, which corresponds to an assumption that turbulence spatial scale lengths (which are assumed to scale with ρ_s) are sufficiently small relative to the equilibrium scale lengths (assumed to scale with a) that the local turbulence and transport characteristics at a given radius depend only upon the local values of the dimensionless parameters which

appear in the GK equations (i.e. $a/L_{T_i} = -a\,\mathrm{d}\ln T_i/\mathrm{d}r$, T_e/T_i, safety factor $q = rB_\phi/RB_\theta$, etc). In the global operation mode, the spatial variation of the dimensionless equilibrium parameters of the GK equation is retained (to lowest order in ρ^*). Differences in predictions between these modes for DIII-D H-mode parameters are discussed in section 3. In all simulations discussed in this paper, the experimental values of ρ^* are used in the numerical simulations.

Unless otherwise noted, all GYRO results presented in this paper were calculated using similar numerical algorithms and resolutions. All simulations include (at a minimum), two ion species: deuterium and carbon, whose dynamics are self-consistently evolved using the GK equations, and electrons described by the drift-kinetic equation (in which only the lowest-order terms in $k_\perp\rho_e$ are retained). Physical box sizes were approximately 100 ρ_s in both the radial and binormal directions. The long radial wavelength components of the toroidially symmetric $n = 0$ fluctuations are weakly damped across the entire domain to ensure the 'net' time-averaged equilibrium profiles remain macroscopically consistent with the input profiles and gradients. Additional damping of the $n = 0$ fluctuations in radial buffer regions 10–20 ρ_s wide (roughly one to two turbulent radial correlation lengths) on either side of the radial domain is applied to eliminate the impact of the Dirichlet boundary conditions on the predictions in the physical domain. The radial grid resolution was 0.4–0.5ρ_s for the β-scan simulations in section 3 and 0.3–0.4ρ_s for the QH-mode simulations in section 4. Twenty toroidal modes with spacing $\Delta n = 5$ were used, spanning the range $0 \leqslant k_\theta\rho_s \leqslant$ 1.1–1.2 at $r/a = 0.6$ corresponding to a binormal mode number resolution $\Delta k_\theta\rho_s = 0.06$ and binormal box size $L_y = 2\pi/\Delta k_\theta \sim 100\rho_s$. A reduced mass ratio $\sqrt{M_i/m_e} = 40$ instead of the physical value of 61 is used, which reduces computational costs associated with resolving the electron dynamics, without significantly impacting the long-wavelength ρ_s-scale dynamics of interest here. A standard 128-point velocity-space discretization is used: (two signs of parallel velocity) × (eight pitch angles) × (eight energies). Collisions are modelled using a pitch-angle scattering operator, evaluated using third- or fifth-order radial basis functions for the QH-mode and β-scan discharges, respectively. Time integration is done using a fixed timestep Runge–Kutta scheme, which combines an implicit treatment of linear electron dynamics with explicit evaluation of the linear ion dynamics and nonlinear terms for all species. The value of the Runge–Kutta integration timestep was $h = 0.005a/c_s$. Finally, all simulations discussed here are electrostatic unless otherwise noted, assuming the both perpendicular and parallel magnetic fluctuations are zero. Even in this electrostatic approximation, finite-β effects related to the magnetic equilibrium such as the Shafranov shift are retained. In all simulations presented below, the turbulent spectrum is found to peak between $k_\theta\rho_s = 0.3$–0.4, with little contribution coming from either the longest or shortest binormal wavenumbers, or from large radial wavenumbers. A pair of simulations for one condition with either the radial resolution or maximum k_θ increased by 50% found less than 20% changes in the predicted transport. We therefore believe that these simulations are sufficiently well converged to draw meaningful conclusions from.

3. Comparisons of gyrokinetic turbulence predictions to DIII-D H-modes with varying β and rotation

Previous studies of idealized [19–22] and experimental [13, 18, 37] cases have shown that for sufficiently small ρ^* (typically of order 0.002), local and global gyrokinetic simulations predict equivalent transport levels. At larger ρ^* values, global simulations are generally found to predict lower transport levels than the local result. Experimentally, the local value of ρ_s is generally found to be small enough at outer radii ($r/a = 0.5$) of typical DIII-D L-modes [38] to support use of the local model. However, closer to the magnetic axis in L-modes, local values of $\rho^* = 0.003$ or greater, leading to differences between local and global predictions at those radii. In most H-modes, the increased confinement leads to increased T_e values, which in turn yield larger local ρ^* values relative to L-modes with comparable magnetic geometries and toroidal fields. These increases can lead to ρ^* values at the outer radii of H-modes that are comparable to the inner radii of L-modes, motivating an assessment of the importance of global effects on gyrokinetic predictions in H-mode cases.

As part of a program to address this issue, local and global simulations of four DIII-D H-mode discharges have been performed. Although these discharges were developed and conducted as part of a study on the effects of transport scaling with $\beta = 8\pi nT/B^2$ at different rotation levels, addressing that issue is not the focus of this initial work, as only electrostatic simulations are considered here. However, these electrostatic studies do represent the baseline results for a currently ongoing investigation into the inclusion of finite magnetic fluctuations at experimentally achievable 'high' β values, the results of which will be presented in future publications. Equilibrium density, temperature, and rotation profiles are shown in figure 1. The four discharges correspond to two-point β scans at low and high rotation, with the β variation achieved via changes in the plasma density ($\bar{n}_e = 4.9 \times 10^{13}$ cm^{-3} and 6.9×10^{13} cm^{-3} respectively at low and high β), toroidal field (scanned from 1.65 T to 1.85 T) and plasma current ($I_p = 1.05$ MA and 1.15 MA, respectively, at low and high β), and heated via mixtures of co- and counter-injected neutral beams. As a convenient shorthand description, each discharge is classified according to whether it has low or high β and low or high rotation (e.g. discharge 128398 would be the 'high β, low-rotation' discharge). However, we emphasize that the nonlinear results shown below are electrostatic; the changes in β only affect the simulation results insofar as they correspond to changes in the underlying equilibrium (e.g. in the Shafranov shift). Finally, consistent with the improved electron thermal confinement of these discharges, each has a local ρ^* value of 0.0035 ± 0.0002 at $r/a = 0.6$, large enough to expect finite differences between local and global predictions.

3.1. Linear growth rate analysis

The local $r/a = 0.6$ linear growth rates of the fastest growing modes in each of the four discharges are plotted in figure 2. In three of the four cases, the ITG mode is the dominant instability at $k_\theta\rho_s < 0.9$, with ITG classification based upon linear real mode frequencies (not shown) in the ion diamagnetic direction.

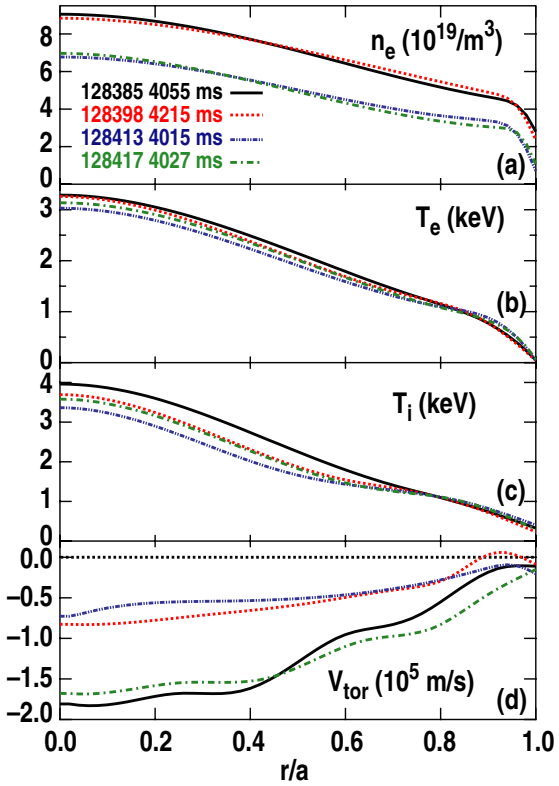

Figure 1. Comparisons of (*a*) electron density n_e, (*b*) electron temperature T_e, (*c*) ion temperature T_i and (*d*) toroidal rotation V_{tor} for four discharges comprising two two-point β scans at low and high rotation.

For the low β, low-rotation discharge (see figure 2(*b*)), trapped electron modes (TEMs) are dominant, based upon linear mode frequencies in the electron direction. The local $E \times B$ shearing rate (calculated using the Waltz–Miller formula [39]) is plotted as a dashed line for each case. In both the low and high rotation cases, the local $E \times B$ shearing rates are approximately equal to the linear growth rate at $k_\theta \rho_s = 0.1$–0.2, and the electrostatic growth rates are well above this shearing rate at higher $k_\theta \rho_s$. In addition to the electrostatic results, the results of including finite perpendicular magnetic fluctuations are also shown. In every case their effect is stabilizing, with only the high β, high rotation case exhibiting a significant reduction at the lower $k_\theta \rho_s$ values where the nonlinear spectrum peaks. Based on these linear results, it seems reasonable to expect that nonlinear electrostatic simulations can provide physically relevant estimates of the turbulence and transport.

3.2. Nonlinear energy flux predictions

The turbulent ion and electron energy fluxes Q_i and Q_e predicted by the nonlinear simulations are shown in figures 3–6. For each case, the input ion and electron temperature profiles (along with corresponding measured data points) are plotted in panels (*a*) and (*b*), respectively, with corresponding predicted ion and electron energy fluxes plotted in panels (*c*) and (*d*), respectively. For each discharge, the predicted fluxes are normalized to the gyroBohm value $Q_{gB} = n_e T_e c_s (\rho^*)^2$, evaluated at $r/a = 0.6$. The explicit inclusion of ρ^* in the normalization reflects that the turbulent fluxes are $O\{(\rho^*)^2\}$ in the gyrokinetic ordering. It also can easily be seen to correspond to the gyroBohm diffusivity $\chi_{gB} = \rho_s^2 c_s / a$, via

$$\frac{Q}{Q_{gB}} = \frac{-n\chi\nabla T}{Q_{gB}} = \left(\frac{n}{n_e}\right)\left(\frac{\chi}{\chi_{gB}}\right)\left(\frac{T}{T_e}\right)\left(\frac{a}{L_T}\right). \quad (1)$$

In these discharges, Q_{gB} evaluated at $r/a = 0.6$ corresponds to physical flux values varying from 4 to 6 W cm^{-2}. This normalization is used rather than physical units to more clearly illustrate the reduced transport levels in H-modes relative to L-modes. In typical DIII-D L-modes, the external heating is generally a factor of two to five smaller than for these H-modes, but the gyroBohm-normalized 'experimental' fluxes (e.g. those calculated via power balance analysis) can be five to ten times larger at $r/a = 0.6$, due to the lower temperatures of the L-modes.

For each of the four discharges modelled, the nonlinear simulations are dominated by the linear ITG or TEM instability identified by the corresponding local simulation. For the ITG-dominated cases (see figures 3, 5 and 6), the global results yield significantly lower predicted energy fluxes than the corresponding local results (plotted as solid circles), ranging from 30% to 50% reductions at $r/a = 0.6$ relative to the local result. The outlier is the TEM-dominated low β, low-rotation case (see figure 4), which shows very close agreement between the local and global transport predictions. In none of the four cases do the global simulations predict larger transport than the corresponding local simulation. All of the simulation results presented here have been run for sufficiently long times that statistical uncertainties in the finite time-averaging are less than 10% of the quoted values (calculated using the approach discussed in Holland *et al* [18]).

The results of power balance calculations of the ion and electron heat fluxes (performed with the ONETWO [40] code) for each discharge are plotted as dashed lines in figures 3–6. The local and global ITG-dominated simulations uniformly overpredict the power balance results when the initial fits to the T_i and T_e measurements (plotted as the solid curves in panel (*a*) of figures 3–6) are taken as the inputs, with the global results generally overpredicting the power balance results by factors of 3–4 in both the ion and electron channels. In contrast, the TEM-dominated simulations underpredict the ion heat flux Q_i by a factor of 2.5 at $r/a = 0.6$, but overpredict Q_e by a factor of 3.

It is well known that plasma turbulence can be quite stiff and sensitive to small changes in input gradients, especially for the low transport levels characteristic of H-mode discharges. To assess the sensitivity of the results to the input gradients, additional global simulation results are plotted in figures 3–6, in which the values of the input normalized ion and electron temperature inverse scale lengths a/L_{T_i} and a/L_{T_e} have been uniformly rescaled across the simulation domain such that the net gyrokinetic energy flux predictions $Q_{net} = Q_i + Q_e$ approximately match the net energy flux calculated via power balance at $r/a = 0.6$. The actual amount of stiffness and sensitivity varies from case to case, but generally changes on the order of 20% to 30% are needed in order to match the energy fluxes. The actual T_i and T_e profiles are self-consistently modified (holding their value at the $r/a = 0.6$ reference value fixed) when a/L_{T_i} and a/L_{T_e} are changed,

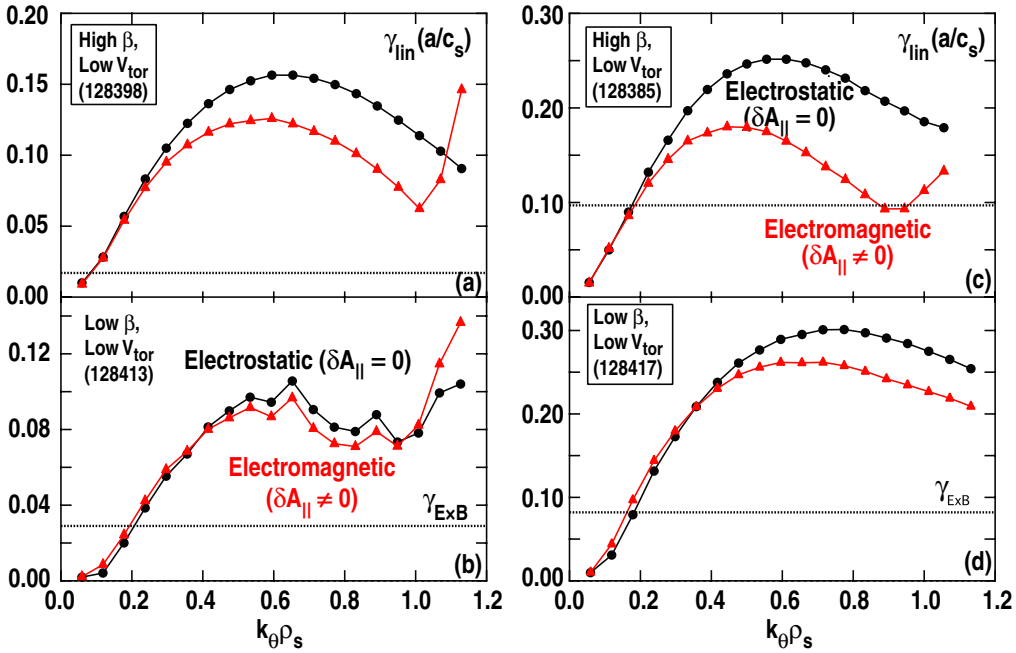

Figure 2. Comparison of electrostatic circles and electromagnetic triangles linear growth rates for modelled β-scan discharges. The low-rotation results are plotted in (a) and (b), for high and low β respectively, while the corresponding high and low β high rotation results are plotted in (c) and (d).

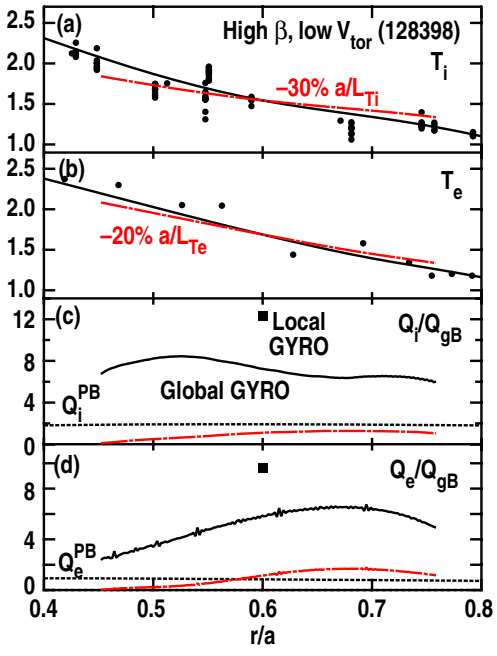

Figure 3. Comparison of measured circles and fitted lines (a) T_i and (b) T_e profiles for the low-rotation, high β discharge (128398). Global predictions of (c) Q_i and (d) Q_e normalized to $Q_\mathrm{gB}(r/a = 0.6)$ (solid lines), and corresponding power balance calculations (dashed curves). Local GYRO flux predictions are squares. The results of flux-matching global simulations are corresponding input T_i and T_e profiles are chained dots.

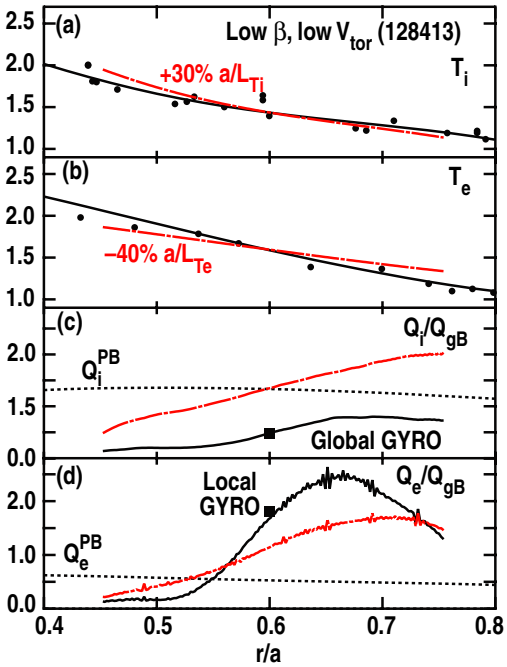

Figure 4. Comparison of measured circles and fitted lines (a) T_i and (b) T_e profiles for the low-rotation, low β discharge (128413). Global predictions of (c) Q_i and (d) Q_e normalized to $Q_\mathrm{gB}(r/a = 0.6)$ (solid lines), and corresponding power balance calculations (dashed lines). Local GYRO flux predictions are squares. The results of flux-matching global simulations are corresponding input T_i and T_e profiles are chained dots.

along with corresponding dimensionless parameters such as $T_\mathrm{e}/T_\mathrm{i}$ and electron–ion collisionality ν_ei. These modified 'flux-matching' profiles are also plotted in panels (a) and (b) figures 3–6, for comparison against the actual profile measurements, and show that even for the largest changes the flux-matching profiles do not differ significantly from the initial profile fits, or more importantly the point profile measurements. For the low β, low-rotation case, these gradient changes lead to ITG-dominated turbulence, rather

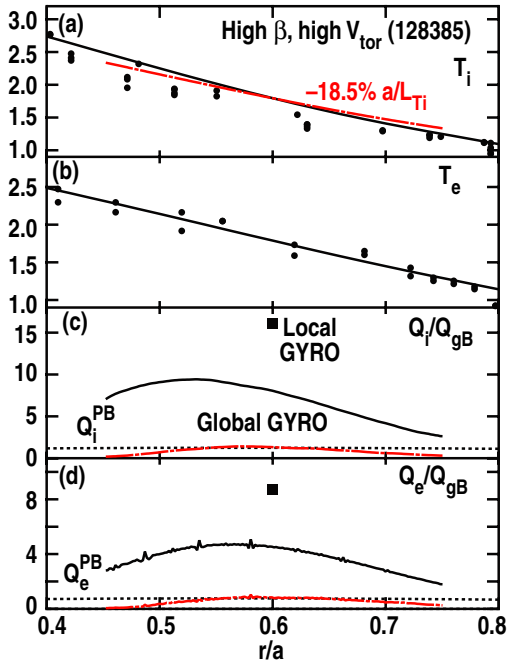

Figure 5. Comparison of measured circles and fitted lines (*a*) T_i and (*b*) T_e profiles for the high rotation, high β discharge (128385). Global predictions of (*c*) Q_i and (*d*) Q_e normalized to $Q_{gB}(r/a = 0.6)$ (solid lines), and corresponding power balance calculations (dashed curves). Local GYRO flux predictions (squares). The results of flux-matching global simulations are corresponding input T_i and T_e profiles (chained dots).

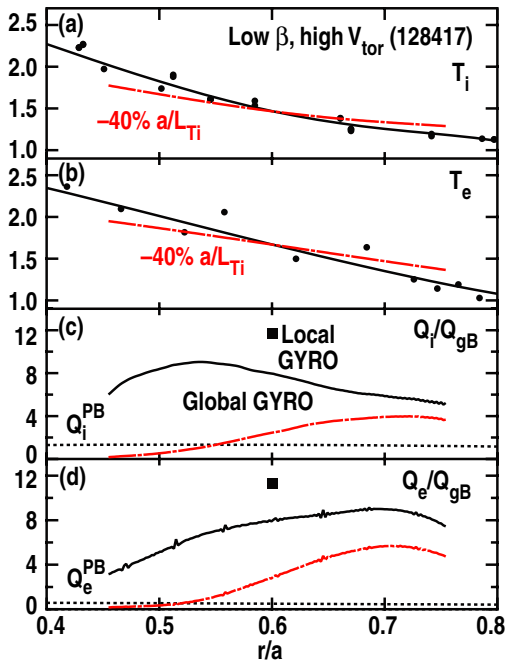

Figure 6. Comparison of measured circles and fitted lines; (*a*) T_i and (*b*) T_e profiles for the high rotation, low β discharge (128417). Global predictions of (*c*) Q_i and (*d*) Q_e normalized to $Q_{gB}(r/a = 0.6)$ (solid lines), and corresponding power balance calculations (dashed curves). Local GYRO flux predictions (squares). The results of flux-matching global simulations are corresponding input T_i and T_e profiles (chained dots).

than the TEM-dominated turbulence found for the initial fits; the other cases remain ITG-dominated. It should be noted that the density and rotation profiles are held fixed in these sensitivity studies, and that in general the particle and momentum fluxes are also over predicted (particularly in the ITG cases), although the lack of accurate calculations of the wall recycling make assessing the exact magnitude of the particle flux overprediction challenging. However, improved flux-matching calculations that varied the density and rotation scale lengths as well as the temperature scale lengths could lead to smaller net changes in a/L_{T_i} and a/L_{T_e}. Inclusion of the stabilizing effect from finite magnetic fluctuations would also lead to smaller changes needed to match the power balance fluxes. Future work will examine these effects, as well as more sophisticated radially dependent modifications of the gradients scale lengths to match the power balance fluxes across the entire simulation domain.

3.3. *Effects of finite collisional damping of* $n = 0$ *fluctuations*

All of the simulation results discussed above include finite ion and electron collisonal damping of the $n = 0$ ('zonal') fluctuations. This damping has been predicted theoretically to be an important turbulence regulation mechanism by reducing zonal flow strength, and thus increasing the strength of the underlying turbulence [41]. However, it is most effective for near-marginal turbulence levels and is in practice negligible for the large normalized turbulence and transport levels characteristic of most of the plasma volume in L-mode discharges, where the experimental energy fluxes can be tens or even hundreds of local gyroBohm units. For the significantly lower transport levels characteristic of H-mode discharges however, it is apparently not a negligible effect. Nonlinear simulations with and without these collisions exhibit statistically significant differences, most pronounced for the TEM-dominated discharge (see figure 7), but still clear for the ITG-dominated systems (see figure 8).

The most surprising result of these comparisons is that this axisymmetric damping clearly has a stronger effect on the electron heat flux Q_e rather than on ion heat flux Q_i. It is not immediately obvious why there is such a difference. The magnitude of the effect also clearly increases with radius, likely reflecting the increase of collisionality with radius. It should be noted that the absolute magnitude of the increase is similar for both the TEM and ITG cases (approximately $0.5\,Q_{gB}$ for Q_i and $2\,Q_{gB}$ for Q_e), but appears as a smaller incremental change in the ITG case because of the significantly higher transport in that scenario. Assuming a similar absolute increase would occur for L-mode plasmas, which have even larger gyroBohm-normalized transport levels, it is not surprising that no clear impact is observed in simulations of those plasmas. Based upon these findings, future efforts focused upon validation of low, near-marginal transport (such as in ITER), should carefully consider the influence of axisymmetric collisional damping upon transport predictions. More generally, the near-marginal low transport levels typical of H-modes will require close attention to any physics or numerical approximations, which can impact the predicted transport values by even a small amount.

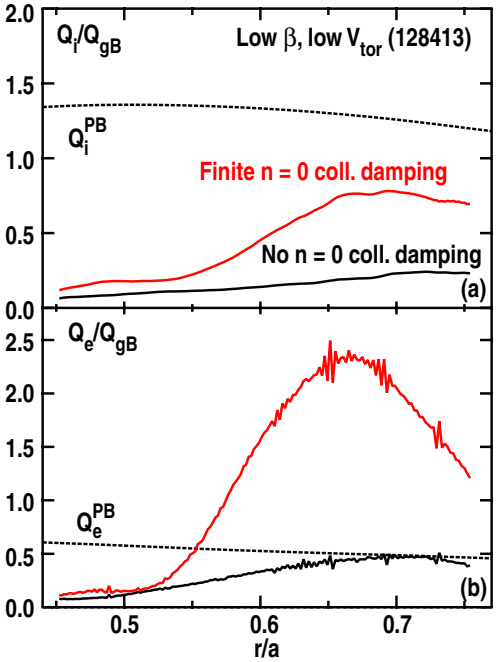

Figure 7. Comparison of global gyrokinetic predictions of (*a*) Q_i and (*b*) Q_e with (—) and without (—) collisional damping of axisymmetric $n = 0$ fluctuations, for a TEM-dominated dominated turbulence. The simulations use the initial profile fits for the low V_{tor}, low β discharge.

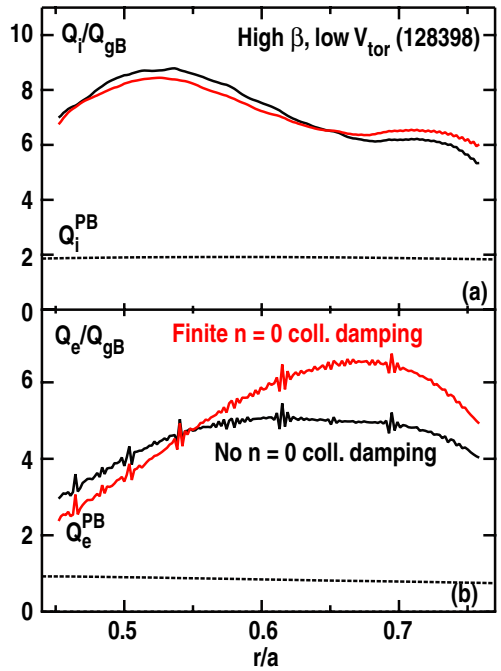

Figure 8. Comparison of global gyrokinetic predictions of (*a*) Q_i and (*b*) Q_e with (-) and without (-) collisional damping of axisymmetric $n = 0$ fluctuations, for ITG-dominated turbulence. The simulations use the initial profile fits for the low V_{tor}, high β discharge.

3.4. Comparison of predicted and measured long-wavelength density fluctuations

In order to robustly validate gyrokinetic model predictions, it is important to go beyond comparisons of transport predictions to power balance calculations (which involve their own modelling and assumptions), and to directly compare predicted fluctuation characteristics against measurements. For such comparisons to be quantitatively meaningful, synthetic diagnostics [13, 14, 42–44] should be applied to the simulation results, to accurately account for the spatiotemporal sensitivities or other characteristics of the diagnostic the model predictions are being compared against. In these discharges, long-wavelength density fluctuations measurements were obtained via far infrared (FIR) scattering [45] and beam emission spectroscopy (BES) [46]. The FIR diagnostic is significantly nonlocal (in that it integrates measurements of fluctuations from a large subvolume of the plasma), and to date, no quantitative synthetic FIR diagnostic suitable for application to microturbulence simulations has been developed. The BES diagnostic on DIII-D yields significantly more localized measurements, with BES measurements in these discharges coming from 30 channels arranged in a 5×6 array in the (R, Z) plane. Each channel has an approximately 1 cm^2 effective integration area in the (R, Z) plane, and the channel to channel spacing is also of order 1 cm in both the radial and vertical directions. For reference, the typical local ρ^* value of 0.0035 at $r/a = 0.6$ in these H-modes correspond to $\rho_s = 2$ mm, as the midplane minor radius a is 60 cm in these plasmas. A synthetic BES diagnostic for use with GYRO and other codes was previously developed [14], and has been used in a variety of studies [11, 14, 16–18]. A common finding in these studies was that the primary effect of the finite spatial volume of the BES diagnostic was to attenuate the physical fluctuation amplitudes by approximately 50%. For instance, applying the synthetic diagnostic to a simulation that predicted long-wavelength density fluctuations with a root-mean-square (RMS) amplitude of 2% would yield synthetic BES fluctuations with 1% RMS amplitude.

Based on these previous findings, we estimate the synthetic BES level predicted by the gyrokinetic simulations as half the locally normalized electron density fluctuation level at the outboard midplane, i.e. as $\delta n_{BES}^{syn} = 0.5 \delta n_e^{GYRO}$. Comparisons of the low-rotation experimental BES results to the global gyrokinetic predictions which used the initial experimental profile fits as inputs are shown in figure 9(*a*), and the results for the flux-matching profiles in figure 9(*b*). Although the predictions made using the initial profile fits are nominally consistent with the measurements (e.g. are of the right magnitude, <1%), the simple synthetic estimate used here clearly does not reproduce the measure levels quantitatively. Perhaps more importantly, these simulations predict a different scaling of fluctuation amplitude with β than is measured, with the fluctuations in the high β discharge predicted to be greater than at small β. In contrast, the flux-matching simulations predict fluctuation levels which are not only quite consistent in magnitude with the measurements, but also reproduce the measured trend of decreasing fluctuation amplitude with increasing β. These results are consistent with previous findings that have demonstrated a close correlation between the level of agreement in GK-predicted and measured fluctuation amplitudes and the level of agreement between the GK-predicted turbulent fluxes and power balance analyses [11–18]. Although BES data for the high rotation discharges

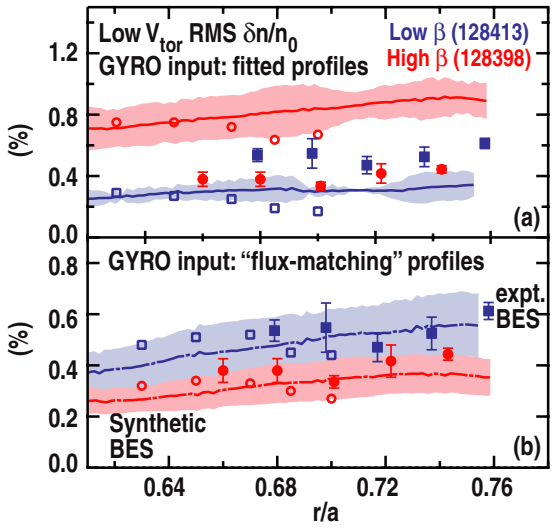

Figure 9. Comparison of BES-measured and synthetic density fluctuation levels for the low-rotation discharges. The model predictions using the initial fits to the T_i and T_e measurements are shown in (*a*), and the predictions of the flux-matching simulations shown in (*b*). The solid symbols correspond to the experimental BES results, and the open symbols to synthetic BES predictions mad using the methodology of [14]. The simple synthetic BES estimates of half the GYRO-predicted midplane RMS density fluctuation amplitudes are plotted as broken lines, with statistical uncertainties denoted by the shading.

are not available directly in the simulated radial domain, they are available at slightly larger radii, and will be compared against model predictions in future work. To provide further weight for these comparisons, 'full' synthetic BES predictions convolving the GYRO density fluctuation predictions with parameter-specific transfer functions using the methodology detailed in Holland *et al* [14] have been calculated for the low-rotation simulations. These improved synthetic calculations show excellent agreement with the simple estimates for both the profile and flux-matching simulations. Because these improved calculations incorporate the full (R, Z) dimensions of the 2D BES array, in which the bottom channels are located 11 cm below the outboard midplane, as well as the magnetic shaping and curvature, the synthetic array must be located at smaller radii than the experimental measurements in order to not extend beyond the physical simulation domain. Despite this limitation, there is still overlap with the experimental measurement locations. In future work, the full synthetic BES algorithms will be used at larger radii in conjunction with improved flux-matching calculations that match the fluxes in all four transport channels (n, T_e, T_i and V_{tor}) across the entire simulation domain.

4. Quantifying the effect of a finite fast ion distribution on turbulence

While H-modes are characterized by the improved confinement and reduced turbulence levels relative to L-modes that are desirable for ITER, most H-modes also exhibit a wide range of macroscopic MHD instabilities and dynamics (such as neoclassical tearing modes and edge localized modes) not present in L-modes, which can make accurate gyrokinetic turbulence simulations that generally do not include nonlinear MHD dynamics challenging. Therefore, the most conclusive gyrokinetic validation tests will likely come from comparisons to time-stationary H-modes in which MHD activity has been eliminated, or at least minimized. Quiescent H-modes (QH-modes) [47, 48] represent such a scenario, in which all core MHD can be eliminated for many hundreds of milliseconds (multiple energy confinement times) while the core profiles remain stationary. Steady pedestal conditions are evidently maintained via the low- [49] to moderate-n [50] coherent modes localized to the outer 10%–20% of the plasma volume. Taking advantage of these capabilities, a dedicated QH-mode validation experiment was performed at DIII-D, which measured transport and turbulence response to changes in the electron heating power in steady-state QH-mode conditions. Initial local, electrostatic GYRO simulations of these discharges were reported in Holland *et al* [18], and found that using standard simulation parameters and model formulation, the gyrokinetic transport predictions exceeded the power balance calculations by an order of magnitude or more. Moreover, these very high-predicted transport levels were found to be remarkably 'unstiff,' and could not be easily reconciled with the power balance calculations for any changes in input temperature, density, or rotation gradients consistent with experimental uncertainties.

In the discussion of these findings in [18], one mechanism identified as a possible source of the discrepancy between the gyrokinetic and power balance results was the neglect of turbulence stabilization due to the significant fast ion fraction. A common characteristic of many QH-modes relative to other H-modes is their relatively low densities; the QH-modes considered in this study had line-averaged electron densities $\bar{n}_e$ of $2.0 \times 10^{13} \pm 5 \times 10^{12}\,\mathrm{cm}^{-3}$. Comparison of the fast neutral beam ion density calculated via the NUBEAM [51] package to the electron density showed that $n_{fast}/n_e \approx 25\%$ in both QH-modes considered at $r/a = 0.6$ (figure 15(*a*) of [18]). Motivated by this observation, a linear growth rate calculation which included the fast ions as a third, independently evolving gyrokinetic ion species (in addition to the deuterium and carbon ions) with a temperature of approximately 35 keV derived from the NUBEAM-calculated beam pressure, exhibited a 50% reduction in the long-wavelength ITG growth rate, relative to the baseline case in which only thermal ions were considered (and the beam ions treated as thermal deuterium ions).

These results are shown in figure 10 and are consistent with previous linear stability results reported by Ernst *et al* in analyses of TFTR 'supershot' discharges [32] and Tardini *et al* [33] for internal transport barriers of ASDEX H-modes. The data in figure 10 also show that the 'pure' dilution assumption, in which an equilibrium thermal deuterium density consistent with the modelled fast particle density is used, but which assumes $\delta f_{fast} = 0$, yields a significantly lower growth rate than the case in which the fast ion fluctuations are not neglected. Thus, there is a clear interaction between the fast ion population and the microturbulence, which has a strong impact on the linear growth rate. Physically, even though $T_{fast} \gg T_e$, there are many 'fast' ions with lower energies which have velocities comparable to c_s and so can still resonantly interact with the turbulence. Apparently, even a weak coupling to the large free energy source represented by the fast ions via these interactions can have significant effect.

An important caveat to these results is that they may well depend sensitively upon the assumption of a

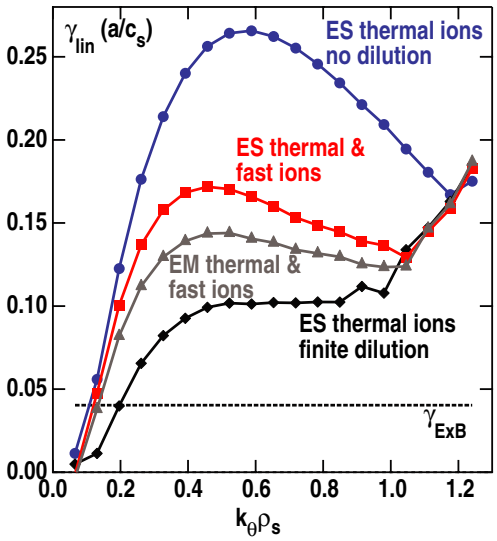

Figure 10. Comparison of linear growth rates for the NBI-only heated QH-mode discussed in [18]. The traces correspond calculations using electrostatic, undiluted thermal ions (circles), electrostatic diluted thermal ions (diamonds), electrostatic thermal and fast ions (squares), and electromagnetic thermal and fast ions (triangles). The increase in growth rates beyond $k_\theta \rho_s = 1$ to 1.2 corresponds to a transition from ITG to TEM modes as the dominant instability at those wavelengths.

Maxwellian distribution of fast beam ions, rather than a more physical anisotropic distribution. The use of the Maxwellian distribution was motivated on both practical grounds (only Maxwellian distributions are currently supported in GYRO) and theoretical (an assumption that the beam ions would not significantly affect the background turbulence due to their high energy) considerations. However, to the extent that the beam ions impact the turbulence via interactions with the low-energy portion of the beam ion distribution, the velocity-space structure of that distribution is clearly important. Previous studies of energetic α-particle transport by Estrada-Mila *et al* [27] and Angioni and Peeters [29] have found that the 'equivalent Maxwellian' approach used here works reasonably well for approximating isotropic (in velocity space) slowing-down distributions. However, the beam ion distribution will be anisotropic in velocity space due to the inherent directed nature of the beam injection (i.e. the beam ions have a mean velocity in the reference frame of the thermal plasma). Moreover, the beam distribution about this mean velocity in non-Maxwellian, nor even necessarily a simple slowing-down distribution, due to the incomplete thermalization of the various beam energy components. To our knowledge, no studies of drift-wave turbulence in the presence of such an anisotropic distribution have been undertaken to date.

Pursuing the hypothesis that an improved fast ion treatment is necessary for accurate predictions of these plasmas further, new local nonlinear simulations of the purely neutral beam-heated QH-mode case discussed in [18] have been performed, quantifying the impact of including this significant beam population on the nonlinear results. The results of these studies are shown in figure 11. Consistent with the linear growth rate analysis of figure 10, inclusion of the fast beam ions as a separate, dynamic species in local electrostatic simulations yields roughly a factor of 1.5 (Q_e) to 2 (Q_t) reduction in predicted transport levels. Inclusion of finite perpendicular magnetic fluctuations $\delta B_\perp = \nabla \times \delta A_\parallel$ in addition to the self-consistent fast ion treatment yields an additional factor of two reduction in transport, for a net factor of four reduction from the electrostatic, thermal ion only simulation. Somewhat surprisingly, inclusion of the magnetic fluctuations without the fast ion population yields an increase in both ion and electron transport. This increase seems to be correlated with an increase in the radial correlation length of the turbulence, and similar effects are seen in local electromagnetic simulations of the β-scan discharges described in section 3 which will be described in future publications. The connection between the finite magnetic effects and correlation length is not yet fully understood, and will be investigated in this future work. As a side note, the significant impact of self-consistently treating the carbon ions is illustrated as well in figure 11, which shows the transport levels predicted by a local electrostatic simulation which evolves only a single (deuterium) ion species with $n_D = n_e$ and retains impurity effects only through inclusion of $Z_{eff} (= 2.7)$ in the electron–ion collisionality rate ν_{ei}. An inconsistent treatment of the carbon ions leads to lower transport predictions; in this discharge the carbon density is in fact strong enough to be a net destabilizing influence, perhaps via destabilization of subdominant TEM modes. It should also be noted that attempts to model this experiment using the adiabatic electrons predict completely shear-suppressed turbulence, highlighting the importance of accurate descriptions of the electron physics for making experimentally relevant transport predictions, even for ITG-dominated plasmas.

While the inclusion of the fast ions (along with electromagnetic stabilization) in and of itself is not enough to reconcile the gyrokinetic and experimental predictions, they do strongly reduce the gyrokinetic predictions, bringing the ion transport to within a factor of 3 of the power balance results. The electron transport remains high in proportional terms, but this result is due more to the near-zero prediction of power balance calculation of the Q_e, rather than the significantly decreased absolute magnitude of the gyrokinetic Q_e prediction. However, as was also noted in the discussion of these results in [18], ρ^* is fairly large for these QH-modes (equal to 0.004 at $r/a = 0.6$), and that consideration of global effects would likely have a strong stabilizing impact as well. In these cases the large ρ^* values means that the 100 ρ^* radial box domain is equivalent to a physical domain encompassing 40% of the plasma radius ($0.4 < r/a < 0.8$). This stabilization was seen in comparisons of local and global simulations of near-axis turbulence in an L-mode discharge with similar ρ^* values in [18], and is also the clear conclusion of the studies in section 3. Moreover, assuming that the reduction of transport due to global effects in these QH-modes would have similar proportional magnitudes as in the other cases, the combination of the stabilizing global effects with the fast ion and electromagnetic effects would likely be sufficient to bring the gyrokinetic and power balance predictions of Q_i into agreement, and would significantly reduce the gyrokinetic Q_e predictions as well. To date, numerical stable and converged global simulations incorporating the fast ion and electromagnetic effects have not been achieved. However, we believe that these results provide a clear and plausible explanation for the large overprediction reported in [18].

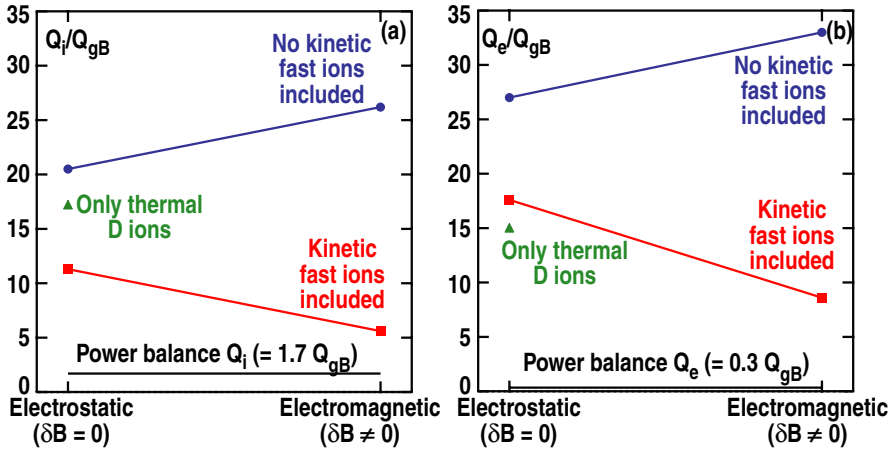

Figure 11. Local GK predictions of (*a*) Q_i and (*b*) Q_e for the NBI-only heated QH-mode discussed in [18]. Model predictions using only thermal deuterium ions (triangles), only thermal deuterium and carbon ions (circles), and thermal deuterium and carbon as well as the fast beam deuterium ions (squares) are shown. The corresponding power balance analyses results are plotted as solid lines.

As a further test of the hypothesis that the fast ions are a key stabilizing mechanism, and that the reported overprediction was not due to some other aspect of the QH-mode operational scenario, additional GYRO simulations of a high-density QH-mode were performed. This discharge has similar heating power to the QH-mode considered above, but a line-averaged density of 4.6×10^{13} cm^{-3}, 2.3 times larger than the initially considered QH-modes, which is achieved by small changes in edge shaping; further experimental details can be found in Burrell *et al* [52]. Equilibrium profiles for this discharge are shown in figure 12. By increasing the density while holding the number of injecting neutral beams fixed, the fast beam ion fraction is reduced from 25% to 5% at $r/a = 0.6$. Nonlinear, local electrostatic GYRO simulations of this discharge at $r/a = 0.6$ were performed, calculating predicted transport levels for various levels of equilibrium $E \times B$ shear with and without treatment of the fast ions as a separate gyrokinetic species; the results are shown in figure 13. In either case, the GYRO predictions are at levels clearly consistent with the power balance results, particularly when the inherent sensitivity and stiffness of the near-marginal transport levels are considered. It is interesting that a clear stabilizing effect is seen when the modest density of fast ions are included, although at these low transport levels this effect may just be due to a small change in the critical gradient(s) for instability induced by the different treatments of the fast ions. The key result is that consistent with the conclusions drawn above, standard gyrokinetic simulations that consider only thermal ions yield reasonable predictions of H-mode transport when the plasma density is sufficiently high that the fast ion fraction is small.

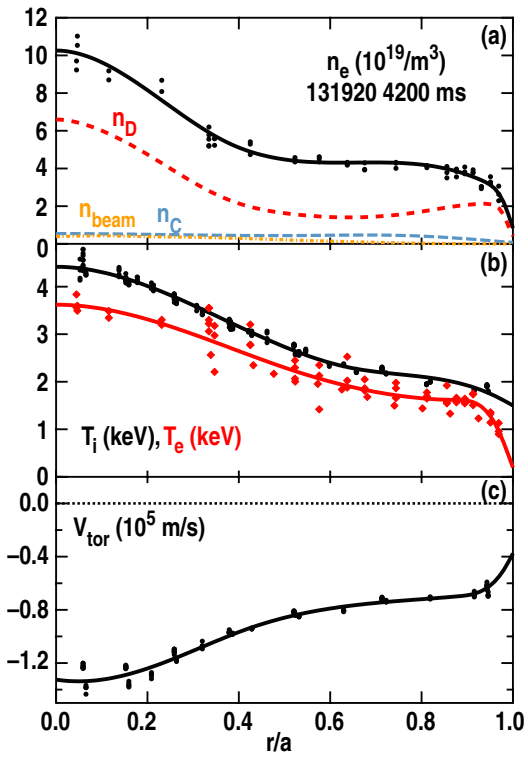

Figure 12. Measured (*a*) n_e, (*b*) T_i and T_e, and (*c*) V_{tor} profiles for a high-density QH-mode (131920). Also plotted in (*a*) are the profiles of the thermal deuterium ions n_D, thermal carbon ions n_c, and fast beam deuterium ions n_{fast}.

5. Differences between H- and L-mode near-edge transport predictions

An important feature of all the H-mode simulations presented here is that there is no evidence for a systematic underprediction of transport at large r/a, as is generally observed for L-mode simulations [14, 17, 18]. If anything, the trend is opposite, towards overpredictions of transport at $r/a > 0.6$–0.7. One hypothesis for this difference lies with the proximity to marginality for the different scenarios, and in a possible breakdown of the GK ordering assumptions in L-modes. As noted above, when normalized to the local gyroBohm value Q_{gB}, the experimental fluxes in H-mode are an order of magnitude smaller than for L-modes. More importantly, the ρ^* ordering used in derivation of the GK and corresponding transport equations assumes that the Q/Q_{gB} should be of order unity, and the H-mode transport levels are well described by this ordering across the entire plasma

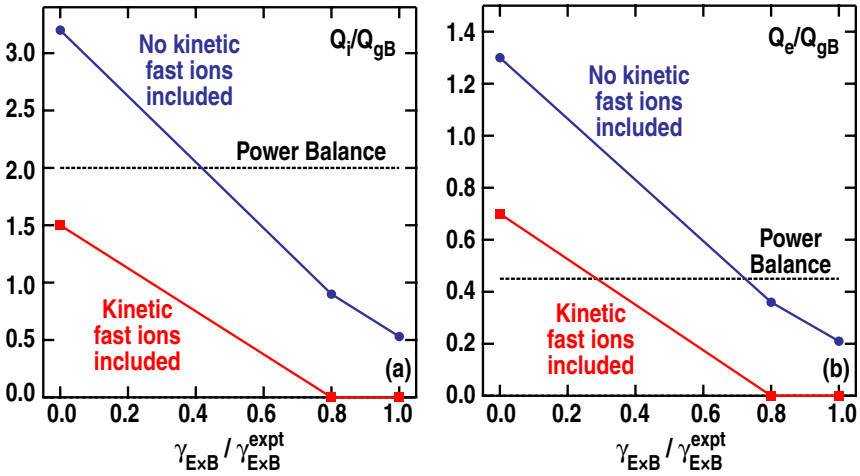

Figure 13. Local, electrostatic GK predictions of (*a*) Q_i and (*b*) Q_e for discharge 131920. Both simulation results using only thermal ions (circles) and, those including the fast beam ion population (squares) are compared against the power balance-calculated fluxes (dashed lines). The results are plotted as a function of the ratio the equilibrium $E \times B$ shear used in the simulation $\gamma_{E\times B}$ to the experimental value of that shear $\gamma^{\mathrm{expt}}_{E\times B}$.

domain to the top of the pedestal. In contrast, the L-mode fluxes increasingly violate this ordering assumption as r/a increases, such that at the larger radii where the prediction shortfall is most pronounced, their normalized fluxes can be on the order of 100–200 [53], approaching a significant fraction of $1/\rho^*$. It is also notable that this ordering breakdown also applies when considering local fluctuation levels (assumed to have amplitudes of order ρ^*), which are generally measured to be less than 1% in H-modes but an order of magnitude larger in the L-mode edge. The significantly better performance of gyrokinetics in explaining transport and turbulence characteristics at smaller radii (e.g. $r/a = 0.5$) in L-modes is also consistent with this hypothesis, as at those radii the normalized fluxes and fluctuation levels are on the order of 5–10Q_gB and $\leqslant$1%, respectively, significantly more in line with the underlying ordering assumptions. A deeper investigation of this issue, comparing model performance to experiment in terms of dimensionless parameters and consistency with ordering assumptions is clearly warranted, and will be undertaken in future work.

6. Conclusions

Confidence in predictions for future devices such as ITER requires that first-principles based models which embody the current state-of-the-art of physics understanding be validated against a wide variety of relevant physical regimes on current-day experiments. Towards this end, gyrokinetic turbulence and transport predictions calculated using the GYRO code were compared against measurements and independent power balance modelling of DIII-D H-mode discharges. These studies focused upon quantifying the nonlocal effects, which can arise at the larger ρ^* values typical of H-modes (relative to L-mode), and on the stabilizing effects of a significant fast beam ion density on the turbulence.

Global, ITG-dominated electrostatic simulations of four H-mode discharges with varying β and rotation exhibited transport levels 30%–50% lower than corresponding local simulations centred at $r/a = 0.6$, while TEM-dominated local and global simulations predicted equal transport levels, as well as lower levels of transport than the ITG cases. The global ITG simulations predicted transport 3–4 times larger than power balance analyses when direct fits to the measured profile data points were input; 20–40% reductions in a/L_{T_i} and or a/L_{T_e} were needed for the gyrokinetic predictions to reproduce the power balance transport calculations at $r/a = 0.6$. 10–20% changes in were required to shift the low β, low-rotation discharge initially predicted to be TEM-dominated into an ITG-dominated regime with transport levels consistent with the corresponding power balance analyses. Although linear analyses suggested that inclusion of finite magnetic fluctuations would generally only have a modest effect on these predictions, they would be expected to stabilize the turbulence relative to these electrostatic levels, and thus lead to smaller required changes to match the power balance results. Future work will address inclusion of these magnetic fluctuations, and improved treatments of the modifications to the input profiles to yield matches to the power balance results across the entire simulation domain. Using a simple synthetic BES estimate that predicts the measured RMS BES amplitude to be half the RMS midplane electron density fluctuation amplitude, the flux-matching simulations of the low-rotation β-scan discharges were shown to reproduce both the absolute measured levels and trend with β, neither of which was reproduced by the simulations using the initial profile fits. More detailed synthetic BES diagnostic calculations, that convolve the predicted density fluctuations with parameter-specific transfer functions using the methodology described in Holland *et al* [14], show excellent agreement with the simple estimates. In future work, simulations at larger radii will also be undertaken to compare with additional BES measurements in both the low and high rotation cases.

A second study focusing upon the effects of turbulence stabilization due to the presence of a significant fast beam ion population provides a resolution for previously reported large overpredictions of power balance transport levels by local GK simulations in QH-mode discharges [18]. It was shown that the significant ($n_\mathrm{fast}/n_\mathrm{e} = 25\%$) beam ion density which can exist

in low $\bar{n}_e$ QH-modes has a strong stabilizing effect, reducing the transport predicted by nonlinear simulations by a factor of two relative to simulations which consider only undiluted, thermal ions. It was also shown that for this discharge (which has $Z_{eff} \sim 2.7$) treating the carbon ions as a separate, dynamic species rather than simply including Z_{eff} in the collisionality leads to quantitatively different predictions of the transport. Furthermore, non-adiabatic electrons are essential for meaningful predictions, even for this ITG-dominated case; the adiabatic electron case yields complete stability rather than the significant overprediction of transport that motivated this study. Simulations of a high $\bar{n}_e$, low fast ion fraction QH-mode exhibited transport levels consistent with power balance analyses, providing further support that the previously reported overprediction was due to the insufficient treatment of the fast ions, rather than a fundamental property of the QH-mode operating regime. When combined with additional stabilization due to electromagnetic fluctuations and nonlocal effects, these results provide a convincing resolution for a previously reported overprediction of QH-mode transport.

Acknowledgments

This work was performed as part of the research program of the Center for Simulation of Plasma Microturbulence. The authors would also like to thank C. Angioni, C. Bourdelle, J. Callen, P.H. Diamond, J.C. DeBoo, D.R. Ernst, W. Guttenfelder, G.W. Hammett, J. Kinsey, D.R. Mikkelsen, W.M. Nevins, R. Prater, S.P. Smith, P.B. Snyder, G.M. Staebler, G.R. Tynan, R.E. Waltz and E. Wang for useful discussions of these results.

This work was supported by the US Department of Energy under DE-FG02-07ER54917, DE-FG02-06ER54871, and General Atomics, University of California, Los Angeles (UCLA), University of Wisconsin, Madison (UW). This research used resources at the National Center for Computational Sciences at Oak Ridge National Laboratory, which is supported by the Office of Science of the Department of Energy under Contract DE-AC05-00OR22725.

References

[1] ITER Physics Expert Groups on Confinement and Transport and Confinement Modeling and Database, ITER Physics Basis Editors and ITER EDA 1999 *Nucl. Fusion* **39** 2175
[2] Horton W. 1999 *Rev. Mod. Phys.* **71** 735
[3] Diamond P.H., Itoh S.-I. and Itoh K. 2010 *Modern Plasma Physics* vol 1 *Physical Kinetics of Turbulent Plasmas* (Cambridge: Cambridge University Press)
[4] Sugama H. and Horton W. 1998 *Phys. Plasmas* **5** 2560
[5] Brizard A.J. and Hahm T.S. 2007 *Rev. Mod. Phys.* **79** 421
[6] Staebler G.M., Kinsey J.E. and Waltz R.E. 2007 *Phys. Plasmas* **14** 055909
[7] Kinsey J.E., Staebler G.M. and Waltz R.E. 2008 *Phys. Plasmas* **15** 055908
[8] Kinsey J.E., Staebler G.M., Candy J., Waltz R.E. and Budny R.V. 2011 *Nucl. Fusion* **51** 083001
[9] Candy J. and Waltz R.E. 2003 *J. Comput. Phys.* **186** 545
[10] Candy J. and Belli E. 2010 GYRO Technical Guide *General Atomics Technical Report* GA-A26818, available at http://www.fusion.gat.com/theory/GYRO
[11] White A.E. *et al* 2008 *Phys. Plasmas* **15** 056116
[12] Casati A. *et al* 2009 *Phys. Rev. Lett.* **102** 165005
[13] Lin L. *et al* 2009 *Plasma Phys. Control. Fusion* **51** 065006
[14] Holland C., White A.E., McKee G.R., Shafer M.W., Candy J., Waltz R.E., Schmitz L. and Tynan G.R. 2009 *Phys. Plasmas* **16** 052301
[15] DeBoo J.C. *et al* 2010 *Phys. Plasmas* **17** 056105
[16] White A.E. *et al* 2010 *Phys. Plasmas* **17** 056103
[17] Rhodes T.L. *et al* 2011 *Nucl. Fusion* **51** 063022
[18] Holland C. *et al* 2011 *Phys. Plasmas* **18** 056113
[19] Waltz R.E., Candy J. and Rosenbluth M.N. 2002 *Phys. Plasmas* **9** 1938
[20] Lin Z., Either S., Hahm T.S. and Tang W.M. 2002 *Phys. Rev. Lett.* **88** 195004
[21] McMillan B.F., Lapillonne X., Brunner S., Villard L., Jolliet S., Bottino A., Görler T. and Jenko F. 2010 *Phys. Rev. Lett.* **105** 155001
[22] Görler T. *et al* 2011 *Phys. Plasmas* **18** 056103
[23] Heidbrink W.W. 2008 *Phys. Plasmas* **15** 055501
[24] Bass E.M. and Waltz R.E. 2010 *Phys. Plasmas* **17** 112319
[25] Zhang H.S., Lin Z., Holod I., Wang X., Xiao Y. and Zhang W.L. 2010 *Phys. Plasmas* **17** 112505
[26] Deng W., Lin Z., Holod I., Wang X., Xiao Y. and Zhang W. 2010 *Phys. Plasmas* **17** 112504
[27] Estrada-Mila C., Candy J. and Waltz R.E. 2006 *Phys. Plasmas* **13** 112303
[28] Hauff T. and Jenko F. 2008 *Phys. Plasmas* **15** 112307
[29] Angioni C. and Peeters A.G. 2008 *Phys. Plasmas* **15** 052307
[30] Angioni C., Peeters A.G., Pereverzev G.V., Bottion A., Candy J., Dux R., Fable E., Hein T. and Waltz R.E. 2009 *Nucl. Fusion* **49** 055013
[31] Zhang W., Decyk V., Holod I., Xiao Y., Lin Z. and Chen L. 2010 *Phys. Plasmas* **17** 055902
[32] Ernst D.R. *et al* 2000 *Phys. Plasmas* **2** 615
[33] Tardini G. *et al* 2007 *Nucl. Fusion* **47** 280
[34] Candy J. 2009 *Plasma Phys. Control. Fusion* **51** 105009
[35] Candy J., Waltz R.E. and Dorland W. 2004 *Phys. Plasmas* **11** L25
[36] Bravenec R.V., Candy J., Barnes M. and Holland C. 2011 *Phys. Plasmas* **18** 122505
[37] Holland C., Candy J., Waltz R.E., White A.E., McKee G.R., Shafer M.W., Schmitz L. and Tynan G.R. 2008 *J. Phys.: Conf. Ser.* **125** 012043
[38] Luxon J.L. 2002 *Nucl. Fusion* **42** 614
[39] Waltz R.E. and Miller R.L. 1999 *Phys. Plasmas* **6** 4265
[40] St. John H.E., Taylor T.S., Lin-Liu Y.R. and Turnbull A.D. 1994 *Plasma Phys. Control. Nucl. Fusion Res.* **3** 603
[41] Diamond P.H., Itoh S.-I., Itoh K. and Hahm T.S. 2005 *Plasma Phys. Control. Fusion* **47** R35
[42] Bravenec R.V. and Nevins W.M. 2006 *Rev. Sci. Instrum.* **77** 015101
[43] Ernst D.R. *et al* 2006 *Proc. 21st Int. Conf. on Fusion Energy 2006 (Chengdu, China, 2006)* (Vienna: IAEA) CD-ROM file TH/1-3 and http://www-naweb.iaea.org/napc/physics/FEC/FEC2006/html/index.htm
[44] Rost J.C., Lin L. and Porkolab M. 2010 *Phys. Plasmas* **17** 062506
[45] Rhodes T.L. *et al* 2006 *Rev. Sci. Instrum.* **77** 10E922
[46] McKee G.R., Fonck R.J., Gupta D.K., Schlossberg D.J., Shafer M.W., Boivin R.L. and Solomon W.M. 2007 *Plasma Fusion Res.* **2** S1025
[47] Greenfield C.M. *et al* 2001 *Phys. Rev. Lett.* **86** 4544
[48] Burrell K.H. *et al* 2005 *Phys. Plasmas* **12** 056121
[49] Snyder P.B. *et al* 2007 *Nucl. Fusion* **47** 961
[50] Yan Z., McKee G.R., Groebner R.J., Snyder P.B., Osborne T.H. and Burrell K.H. 2011 *Phys. Rev. Lett.* **107** 055004
[51] Pankin A., McCune D., Andre R., Bateman G. and Kritz A. 2004 *Comput. Phys. Commun.* **159** 157
[52] Burrell K.H. *et al* 2009 *Nucl. Fusion* **49** 085024
[53] Candy J., Holland C., Waltz R.E., Fahey M.R. and Belli E. 2009 *Phys. Plasmas* **16** 060704